

Fluorinated Carbonate Electrolyte with Superior Oxidative Stability Enables Long-Term Cycle Stability of $\text{Na}_{2/3}\text{Ni}_{1/3}\text{Mn}_{2/3}\text{O}_2$ Cathodes in Sodium-Ion Batteries

Shuilin Wu, Bizhe Su, Kun Ni, Fei Pan, Changlai Wang, Kaili Zhang, Denis Y. W. Yu,* Yanwu Zhu,* and Wenjun Zhang*

Layered transition metal oxides are promising cathode materials for sodium-ion batteries applicable for low-cost energy storage systems. However, their cycle stability needs to be substantially improved to meet the requirements of practical applications. Specifically, the issues related to electrolyte stability and the formation of an unstable cathode–electrolyte interface (CEI) remain unsolved. Herein, it is shown that an electrolyte with high fluorine content may induce a robust fluorinated CEI on $\text{Na}_{2/3}\text{Ni}_{1/3}\text{Mn}_{2/3}\text{O}_2$ cathode, a representative transitional metal oxide, which can efficiently passivate its surface and suppress continuous electrolyte decomposition during cycling. As a result, the cells deliver a remarkably improved rate capability and cycle stability. Density functional simulations further validate the superior stability of fluorinated electrolyte on cathodes with low highest occupied molecule orbital energy and high dissociation energy barriers. This finding demonstrates the favorable role of fluorinated electrolytes for improving the long-term cycle stability of $\text{Na}_{2/3}\text{Ni}_{1/3}\text{Mn}_{2/3}\text{O}_2$ cathode toward grid-scale applications.

1. Introduction

With the merits of high abundance and low cost of sodium, sodium-ion batteries (SIBs) are emerging as a promising alternative to Li ion batteries, especially for applications in large-scale grid energy storage systems.^[1,2] In the development of SIBs, various cathode materials have been extensively studied, such as transition metal oxides,^[3–9] Prussian blue and its analogues,^[10–12] polyanionic compounds,^[13,14] and organic compounds;^[15–17] and the design of cathode materials has shown great impact on the performance of SIBs, for example, energy density, power density, and cycle stability. Among these materials, some layered transition metal oxides, with $\text{Na}_{2/3}\text{Ni}_{1/3}\text{Mn}_{2/3}\text{O}_2$ as a representative, have intriguing characteristics including high theoretical specific capacity, low cost, and inertness

against moisture.^[18,19] Nevertheless, the poor structural durability of $\text{Na}_{2/3}\text{Ni}_{1/3}\text{Mn}_{2/3}\text{O}_2$ during sodiation/de-sodiation processes is still a challenge for improving the stability of SIBs toward practical applications, and various strategies have been employed to tackle this challenge.^[20–26] For example, Guo and co-workers reported that substituting partial Mn sites with Ti in $\text{Na}_{2/3}\text{Ni}_{1/3}\text{Mn}_{2/3}\text{O}_2$ could stabilize the cathodes during cycling and thus enable a capacity retention of 84% after 500 cycles.^[27] Zhou and co-workers stabilized $\text{Na}_{2/3}\text{Ni}_{1/3}\text{Mn}_{2/3}\text{O}_2$ cathode with an Al_2O_3 protection coating layer, achieving a capacity retention of 73% after 300 cycles.^[25] Moreover, through optimizing the range of operating voltage within 1.5–4.0 V, Fan and co-workers revealed that the phase-transition of $\text{Na}_{2/3}\text{Ni}_{1/3}\text{Mn}_{2/3}\text{O}_2$ during cycling could be effectively avoided, resulting in a high capacity retention of up to 81% after 500 cycles.^[24]


Although the previous works have shown improved cycle performance of $\text{Na}_{2/3}\text{Ni}_{1/3}\text{Mn}_{2/3}\text{O}_2$, the effects of electrolyte decomposition and cathode–electrolyte interface (CEI) on the cycle stability of $\text{Na}_{2/3}\text{Ni}_{1/3}\text{Mn}_{2/3}\text{O}_2$ remain unclear.^[28] In particular, the CEI will inevitably crack and reform due to the volume change of $\text{Na}_{2/3}\text{Ni}_{1/3}\text{Mn}_{2/3}\text{O}_2$ during cycling, while electrolyte is continuously consumed with irreversible extraction of Na^+ ions from the $\text{Na}_{2/3}\text{Ni}_{1/3}\text{Mn}_{2/3}\text{O}_2$ material. Such influences will be exacerbated with prolonged cycles, for example,

Dr. S. Wu, Dr. C. Wang, Prof. W. Zhang
Department of Materials Science and Engineering
& Center of Super-Diamond and Advanced Films
City University of Hong Kong
83 Tat Chee Avenue, Hong Kong, China
E-mail: apwjzh@cityu.edu.hk

B. Su, Dr. D. Y. W. Yu
School of Energy and Environment
City University of Hong Kong
83 Tat Chee Avenue, Hong Kong, China
E-mail: denisyu@cityu.edu.hk

Dr. K. Ni, Dr. F. Pan, Prof. Y. Zhu
Hefei National Research Center for Physical Sciences at the Microscale
& Department of Materials Science and Engineering
& CAS Key Laboratory of Materials for Energy Conversion
& i-CHEM
University of Science and Technology of China
Hefei, Anhui 230026, China
E-mail: zhuyanwu@ustc.edu.cn

Prof. K. Zhang
Department of Mechanical Engineering
City University of Hong Kong
83 Tat Chee Avenue, Hong Kong, China

 The ORCID identification number(s) for the author(s) of this article can be found under <https://doi.org/10.1002/aenm.202002737>.

DOI: 10.1002/aenm.202002737

over thousand cycles, and greatly shorten the lifetime of the batteries. Thus, the formation of a robust CEI and the use of a stable electrolyte are also essential to promote the long-term cycle stability of $\text{Na}_{2/3}\text{Ni}_{1/3}\text{Mn}_{2/3}\text{O}_2$.

Till now, there have been only a few studies on the formation of CEI on SIB cathode surface, as compared with solid-electrolyte interface formed on the anode side, partly because the volume change of most cathodes during cycling is smaller than that of anodes, and the operating voltages are in general below the oxidation potential of electrolytes.^[29] However, for cathodes containing transition metal elements, such as $\text{Na}_{2/3}\text{Ni}_{1/3}\text{Mn}_{2/3}\text{O}_2$, oxidative decomposition of electrolytes could probably be induced even at an operation voltage lower than the oxidation potential of electrolytes due to the higher catalytic activity of transition metals. Besides, even though the volume change of cathodes during sodiation/de-sodiation is relatively small, it can still exert a large accumulated stress on the CEI induced by repeated volume change after prolonged cycles, which results in the cracking of the CEI and acceleration of electrolyte decomposition. Thus, an electrolyte which is stable even at a higher operation voltage and enables the formation of a robust CEI will be favorable for achieving long-term cycle stability of cathodes. As compared with common carbonate solvents, fluorinated carbonates theoretically have lower highest occupied molecular orbital (HOMO) energy and therefore are more stable against oxidation on cathodes.^[30,31] Recently, fluoroethylene carbonate (FEC) has been utilized as an additive (3–5 wt%) in the electrolyte, and improved performances of cathodes to a certain extent were demonstrated in SIBs.^[18,24,25] Nevertheless, it is unclear how the FEC additive in electrolyte affects the formation of CEI because FEC is theoretically more stable than common carbonates at the cathode side, and such small amounts of FEC cannot ensure the long-term cycle stability after its depletion.

In this work, the effects of the fluorinated electrolyte, that is, 1 M NaClO_4 in FEC (termed as FEC electrolyte), on improving the electrochemical performance of $\text{Na}_{2/3}\text{Ni}_{1/3}\text{Mn}_{2/3}\text{O}_2$ cathodes in SIBs were systematically studied. It is revealed that the FEC leads to the formation of a robust fluorinated CEI on $\text{Na}_{2/3}\text{Ni}_{1/3}\text{Mn}_{2/3}\text{O}_2$ that efficiently passivates the cathode surface. Thus, the robust fluorinated CEI suppresses the continuous electrolyte decomposition and prohibits excessive formation of the CEI, ensuring an efficient transport of Na ions through the surface even with prolonged cycles. As a result, $\text{Na}_{2/3}\text{Ni}_{1/3}\text{Mn}_{2/3}\text{O}_2$ cathode demonstrates excellent rate capability (86% capacity retention when current density is increased from 0.2 to 30 C) and remarkable cycle stability (87% capacity retention after 2000 cycles at 5 C) in the FEC electrolyte, which is superior to the performances obtained in other typical fluorine-free carbonate-based electrolytes. Density functional simulations further show that FEC molecule is more stable on the cathode side with lower HOMO energy and higher dissociation energy barriers than propylene carbonate (PC) molecule. Furthermore, a full cell was constructed by using $\text{Na}_{2/3}\text{Ni}_{1/3}\text{Mn}_{2/3}\text{O}_2$ as cathode and commercial hard carbon as anode in FEC electrolyte; and its excellent performance (e.g., 94% capacity retention after 1000 cycles at 5 C, and 88% capacity retention when current density is increased from 0.3 to 10 C) further validates the feasibility of using electrolytes with fluorinated carbonates as solvents for practical application.

2. Results and Discussion

The $\text{Na}_{2/3}\text{Ni}_{1/3}\text{Mn}_{2/3}\text{O}_2$ cathodes were prepared through a facile solid-state reaction (as described in the experiment section in supporting information); and the phase of $\text{Na}_{2/3}\text{Ni}_{1/3}\text{Mn}_{2/3}\text{O}_2$ was verified by X-ray diffraction (XRD) and transmission electron microscopy (TEM), as shown in Figure S1, Supporting Information. To evaluate the effects of FEC solvent on the cathode performance, $\text{Na}_{2/3}\text{Ni}_{1/3}\text{Mn}_{2/3}\text{O}_2$ -Na cells were assembled using the FEC electrolyte and other typical fluorine-free carbonates, for example, PC, ethylene carbonate/dimethyl carbonate (EC/DMC), EC/PC, and ethylene carbonate/diethyl carbonate (EC/DEC) as control. The ionic conductivity and viscosity of these electrolytes was measured and the results are shown in Figure S2, Supporting Information. Specifically, the ionic conductivity is in the sequence of EC/DMC > EC/PC > EC/DEC > PC > FEC, while the viscosity is in the sequence of FEC > PC > EC/PC > EC/DEC > EC/DMC. Despite the lowest ionic conductivity yet highest viscosity, the FEC electrolyte still enables the best electrochemical performance (e.g., rate capability, Coulombic efficiency, and cycle stability) as discussed below. This result indicates that ionic conductivity and viscosity of the electrolytes are not major factors affecting the electrochemical performance in this work. Similar voltage–capacity curves were obtained for all cells, as presented in Figure 1a and Figure S3a–c, Supporting Information, indicating the same sodiation/de-sodiation processes of $\text{Na}_{2/3}\text{Ni}_{1/3}\text{Mn}_{2/3}\text{O}_2$ cathodes in these electrolytes. However, the cell with FEC electrolyte delivers an obviously higher Coulombic efficiency for the initial cycles, as compared with the cells in fluorine-free carbonate-based electrolytes (Figure S3d, Supporting Information). The observation of the highest Coulombic efficiency from the cell with FEC electrolyte among all cells suggests superior stability of FEC on the surface of $\text{Na}_{2/3}\text{Ni}_{1/3}\text{Mn}_{2/3}\text{O}_2$ cathode that suppresses side reactions and electrolyte decomposition during the sodiation/de-sodiation processes. Moreover, the superior stability of FEC electrolyte is also supported by the smaller currents at high voltage range in the cyclic voltammograms of $\text{Na}_{2/3}\text{Ni}_{1/3}\text{Mn}_{2/3}\text{O}_2$ -Na and Na–Al cells with FEC electrolyte (Figures S4 and S5, Supporting Information). The linear scan voltammograms of Na–Al cells with FEC and PC electrolytes (Figure S6, Supporting Information) also verified the superior cathodic stability of FEC electrolyte. The cell with FEC electrolyte demonstrates excellent long-term cycle stability with 87% capacity retention after 2000 cycles, outperforming cells with other electrolytes (Figure 1b and Figure S7, Supporting Information). From the voltage–capacity curves at prolonged cycles (Figures S8 and S9, Supporting Information), the polarization increases much slower in the cell with FEC electrolyte than that in cells with other electrolytes. The rapidly increasing polarization in fluorine-free carbonate-based electrolytes with cycling is attributed to successive decomposition of electrolyte and the formation of excessive CEI that blocks the Na^+ transportation.^[32] This is consistent with rate performance tests, where cells with FEC electrolyte also show outstanding rate capability (Figure 1c) and low polarization at different current densities (Figure 1d,e).

Scanning electron microscopy (SEM) was employed to investigate the change in appearance of the $\text{Na}_{2/3}\text{Ni}_{1/3}\text{Mn}_{2/3}\text{O}_2$ cathode surface after different cycles (e.g., 300th, 1000th, and 2000th cycles) and the pristine electrode was also tested for

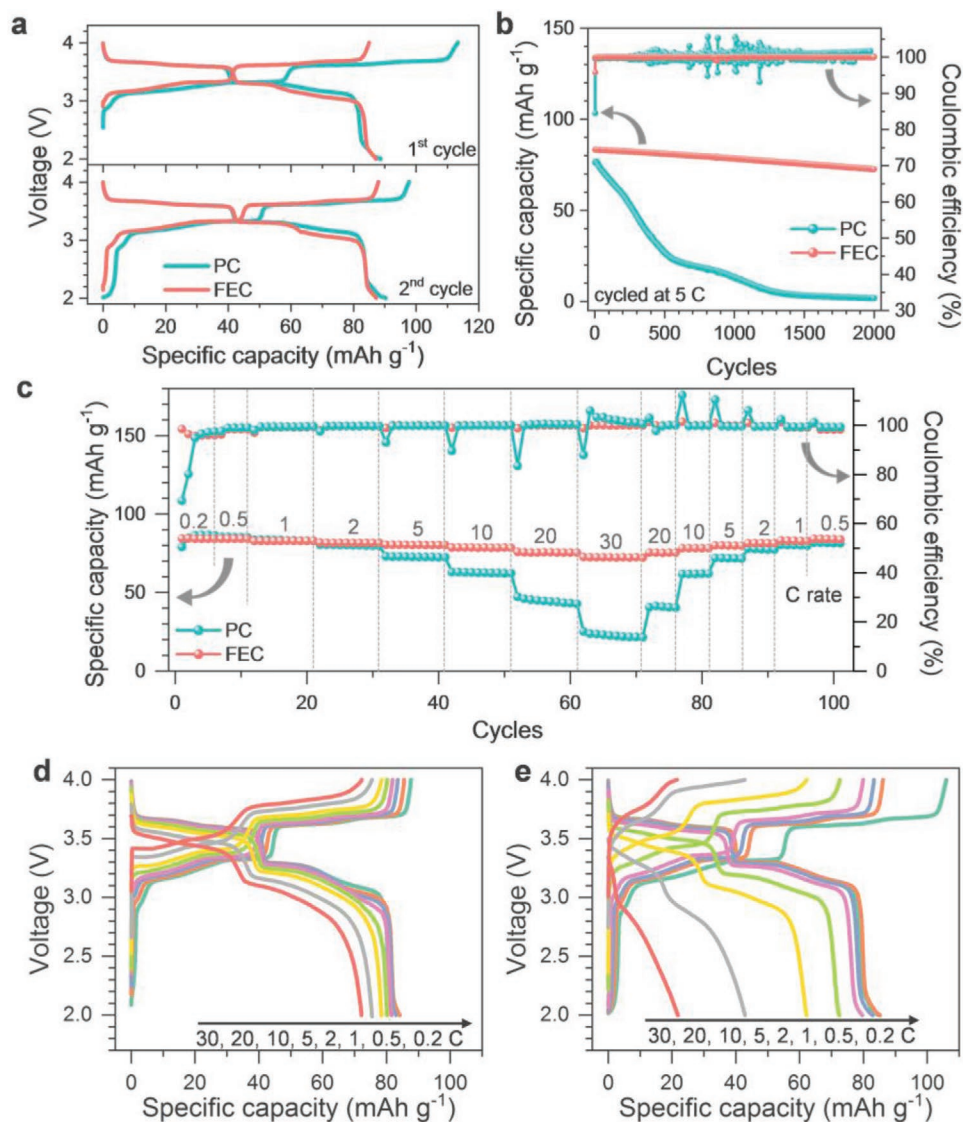


Figure 1. Electrochemical performance of $\text{Na}_{2/3}\text{Ni}_{1/3}\text{Mn}_{2/3}\text{O}_2\text{-Na}$ cells cycled with PC and FEC electrolytes, respectively. a) The voltage–capacity curves of the first two cycles at 0.3 C ($1\text{ C} = 80\text{ mA g}^{-1}$). b) The cycle stability of $\text{Na}_{2/3}\text{Ni}_{1/3}\text{Mn}_{2/3}\text{O}_2$ at 5 C. c) The rate performance of $\text{Na}_{2/3}\text{Ni}_{1/3}\text{Mn}_{2/3}\text{O}_2$ from 0.2 to 30 C. The voltage–capacity curves of $\text{Na}_{2/3}\text{Ni}_{1/3}\text{Mn}_{2/3}\text{O}_2$ cycled in d) FEC and e) PC electrolytes at different current densities (0.2–30 C).

reference in Figure S10, Supporting Information. In cells with electrolyte of 1M NaClO_4 in PC (termed as PC electrolyte), the surface of the $\text{Na}_{2/3}\text{Ni}_{1/3}\text{Mn}_{2/3}\text{O}_2$ cathode is covered with a semi-transparent CEI layer after 300 cycles (Figure 2a). The appearance of $\text{Na}_{2/3}\text{Ni}_{1/3}\text{Mn}_{2/3}\text{O}_2$ grains becomes more obscure with prolonged cycles as the CEI thickens (as discussed below) (Figure 2b,c), which is attributed to the continuous decomposition of electrolyte. Moreover, after 2000 cycles, cracks are observed on the $\text{Na}_{2/3}\text{Ni}_{1/3}\text{Mn}_{2/3}\text{O}_2$ grains, which may be attributed to the accumulatively irreversible extraction of Na from $\text{Na}_{2/3}\text{Ni}_{1/3}\text{Mn}_{2/3}\text{O}_2$ with continuous electrolyte decomposition (Figure 2c and Figure S11a, Supporting Information). The continuous consumption of electrolyte and crack of $\text{Na}_{2/3}\text{Ni}_{1/3}\text{Mn}_{2/3}\text{O}_2$ grains accelerate the capacity decay of the cells with PC electrolyte. In comparison, the $\text{Na}_{2/3}\text{Ni}_{1/3}\text{Mn}_{2/3}\text{O}_2$ grains in the cells with FEC electrolyte can still be clearly seen

after 2000 cycles (Figure 2d–f). Besides, close observations by TEM also reveal that the $\text{Na}_{2/3}\text{Ni}_{1/3}\text{Mn}_{2/3}\text{O}_2$ grains maintain intact even after 2000 cycles (Figure S11b, Supporting Information). Moreover, the XRD patterns (Figure S12, Supporting Information) and Raman spectra (Figure S13, Supporting Information) of the $\text{Na}_{2/3}\text{Ni}_{1/3}\text{Mn}_{2/3}\text{O}_2$ after 2000 cycles were the same with those of pristine electrodes, revealing that the differences of the electrochemical performance were ascribed to the electrolyte stability and corresponding CEI formation. These results imply that the use of FEC electrolyte improves the stability against oxidation and effectively restrains the successive formation of CEI on the $\text{Na}_{2/3}\text{Ni}_{1/3}\text{Mn}_{2/3}\text{O}_2$ surface.

The chemical composition of the CEI layer on $\text{Na}_{2/3}\text{Ni}_{1/3}\text{Mn}_{2/3}\text{O}_2$ cathodes was further investigated by X-ray photo-electron spectroscopy (XPS) and the corresponding atomic ratio was calculated in Table S1, Supporting

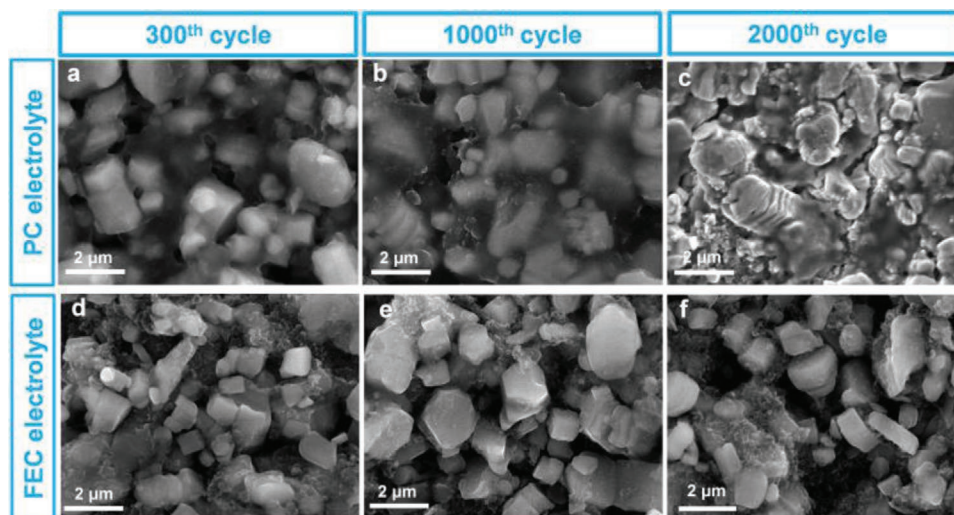


Figure 2. SEM images of $\text{Na}_{2/3}\text{Ni}_{1/3}\text{Mn}_{2/3}\text{O}_2$ cathodes after 300, 1000, and 2000 cycles at 5 C in a–c) PC electrolyte and d–f) FEC electrolyte.

Information. The C 1s spectrum of $\text{Na}_{2/3}\text{Ni}_{1/3}\text{Mn}_{2/3}\text{O}_2$ cathode cycled in the FEC electrolyte is similar to that of pristine $\text{Na}_{2/3}\text{Ni}_{1/3}\text{Mn}_{2/3}\text{O}_2$ cathode (Figure 3a), where the peaks are ascribed to common carbonaceous groups, such as C–C (284.3 eV), C–O (285.5 eV), C=O (287.4 eV), and C–F (290.0 eV). In contrast, the $\text{Na}_{2/3}\text{Ni}_{1/3}\text{Mn}_{2/3}\text{O}_2$ cathode cycled in the PC electrolyte shows a higher intensity of the peaks assigned to C=O and C–O groups, which is considered to be ascribed to the decomposition of electrolyte. For the O 1s spectra (Figure 3b), the $\text{Na}_{2/3}\text{Ni}_{1/3}\text{Mn}_{2/3}\text{O}_2$ cathode cycled in the FEC electrolyte exhibits a slightly decreased peak intensity

assigned to metal–oxygen bond (M–O, ≈ 530.0 eV) and higher peak intensity assigned to C–O group (≈ 531.0 eV), in comparison with that of pristine $\text{Na}_{2/3}\text{Ni}_{1/3}\text{Mn}_{2/3}\text{O}_2$ electrode. Besides, a weak peak (535.6 eV) ascribed to O–F bonds is observed on the $\text{Na}_{2/3}\text{Ni}_{1/3}\text{Mn}_{2/3}\text{O}_2$ cathode cycled in FEC electrolyte. For the $\text{Na}_{2/3}\text{Ni}_{1/3}\text{Mn}_{2/3}\text{O}_2$ cathode cycled in PC electrolyte, only two peaks assigned to C–O and C=O groups are observed in the O 1s spectrum. Such results disclose that both PC and FEC solvents undergo decomposition on the $\text{Na}_{2/3}\text{Ni}_{1/3}\text{Mn}_{2/3}\text{O}_2$ cathode, and the decomposition of PC is more severe than that of FEC. Besides, the F 1s spectra (Figure 3c) and its high atomic

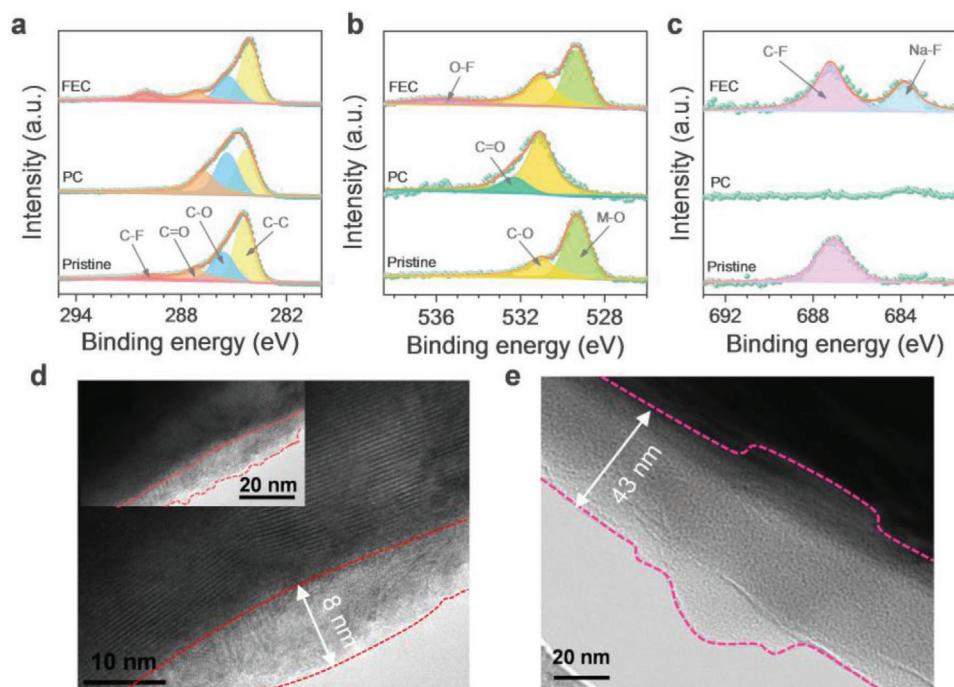


Figure 3. Characterization of the CEI on the $\text{Na}_{2/3}\text{Ni}_{1/3}\text{Mn}_{2/3}\text{O}_2$ cathodes in PC and FEC electrolytes. XPS spectra of $\text{Na}_{2/3}\text{Ni}_{1/3}\text{Mn}_{2/3}\text{O}_2$ cathodes; a) C 1s spectra, b) O 1s spectra, and c) F 1s spectra. The corresponding TEM images of $\text{Na}_{2/3}\text{Ni}_{1/3}\text{Mn}_{2/3}\text{O}_2$ cathodes cycled in d) FEC electrolyte and e) PC electrolyte.

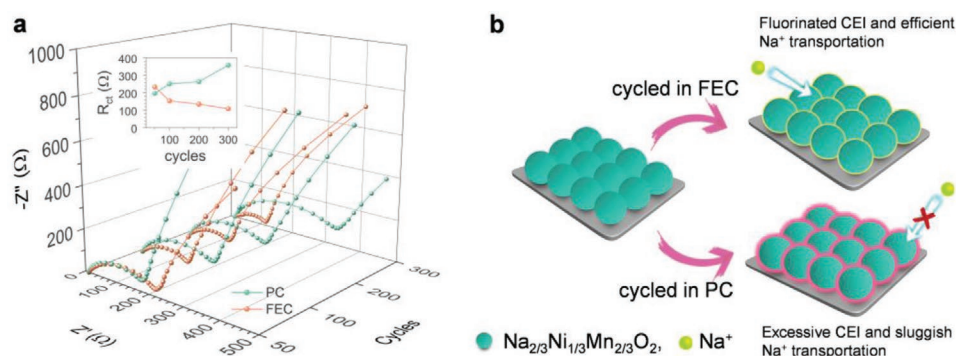


Figure 4. Electrochemical impedance spectra of $\text{Na}_{2/3}\text{Ni}_{1/3}\text{Mn}_{2/3}\text{O}_2$ cathodes and corresponding schematic illustration. a) The Nyquist curves of electrodes after 50, 100, 200, and 300 cycles at 5 C in FEC and PC electrolytes. The inset summarizes the charge transfer resistances of the electrodes after different cycles. b) Schematic illustration of the CEI formation on $\text{Na}_{2/3}\text{Ni}_{1/3}\text{Mn}_{2/3}\text{O}_2$ grains after cycling in FEC and PC electrolytes.

content (Table S1, Supporting Information) indicate that FEC formed a fluorinated CEI on the $\text{Na}_{2/3}\text{Ni}_{1/3}\text{Mn}_{2/3}\text{O}_2$ cathode. TEM images further reveal a much thinner CEI layer formed on the $\text{Na}_{2/3}\text{Ni}_{1/3}\text{Mn}_{2/3}\text{O}_2$ cathode after 10 cycles at 0.3 C in FEC electrolyte (≈ 8 nm, Figure 3d) than that formed in PC electrolyte (≈ 43 nm, Figure 3e). Based on the XPS and TEM results above, it can be concluded that the CEI layers in both PC and FEC electrolytes are derived from electrolyte decomposition, and the fluorinated CEI layer formed in the FEC electrolyte is thinner and more stable than that formed in PC electrolyte, which reduces the excessive decomposition of the electrolyte and enables a much improved cycle stability of the cathodes.^[30,32,33]

To verify this conclusion, electrochemical impedance spectroscopy (EIS) was also conducted to study the impedance variation of the samples after 50, 100, 200, and 300 cycles at the fully discharged state. From the Nyquist curves (Figure 4a), the interfacial resistance of the cells with FEC electrolyte after 50 cycles is 234 Ω, slightly higher than that of the cells with PC electrolyte (197 Ω). With increasing cycles, the interfacial resistances of the cells with FEC electrolyte decrease to 154, 135, and 109 Ω after 100, 200, and 300 cycles, respectively; whereas the interfacial resistances of the cells with the PC electrolyte increase to 251, 264, and 358 Ω, respectively, under the same condition. The gradual decrease in interfacial resistance of the half cells with FEC electrolyte is consistent with the small change in polarization with prolonged cycles (Figure S8a, Supporting Information). In contrast, the increased interfacial resistances of the cells with PC electrolyte are associated with the considerably raised polarization after prolonged cycles as shown in Figure S8b, Supporting Information. Moreover, the slope of the linear region in the Nyquist curves of the cells with the FEC electrolyte slightly increased and then maintained unchanged after 100 cycles, indicating that the ion diffusivity does not change much. In contrast, the slope of the linear region in the Nyquist curves of the cells with the PC electrolyte gradually decreased with prolonged cycles, revealing a decrease in ion diffusivity. This is also consistent with the reaction of PC electrolyte with the electrode with increased cycles. Besides, the galvanostatic intermittent titration technique was employed to study the diffusion kinetics of Na^+ cations in bulk phase and the results depicted the same diffusion kinetics in bulk phase during charging/discharging process in PC and FEC electrolytes with the similar

curves (Figure S14, Supporting Information). The cycle stability of $\text{Na}_{2/3}\text{Ni}_{1/3}\text{Mn}_{2/3}\text{O}_2$ was also evaluated in PC electrolyte with different contents of FEC at 0.5 and 5 C, respectively; and the results showed that the cycle stability of the cells increased with the FEC content (Figures S15 and S16, Supporting Information). Herein, the continuous decomposition of the PC electrolyte on the $\text{Na}_{2/3}\text{Ni}_{1/3}\text{Mn}_{2/3}\text{O}_2$ surface results in a thick CEI layer that blocks Na^+ transportation, finally causing sluggish kinetics and accelerating capacity decay (Figure 4b, bottom panel). On the contrary, the FEC electrolyte induces the formation of a robust fluorinated CEI that can effectively passivate the cathode surface and suppress further decomposition of electrolyte, and ensures long-term cycle stability and excellent rate performance due to the rapid Na^+ transportation through the CEI, as illustrated in Figure 4b (upper panel).^[34,35]

To understand the origin of the superior stability of FEC electrolyte on the cathode side, simulations based on density functional theory (DFT) in combination with ab-initio molecular dynamics (AIMD) were conducted. The detailed simulation methods are described in the Experiment Section, Supporting Information. Based on the AIMD results under the NVT ensemble, the solvation structures of 1 M NaClO_4 in FEC and PC were investigated and the pair distribution functions ($g(r)$) of Na–O and Na–O&F pairs are summarized in Figure 5a. By integrating $g(r)$ in the first contact layer, the coordination number of Na–O pairs in PC is estimated to be ≈ 5 , and the coordination number of Na–O and Na–F pairs together in FEC is calculated to be ≈ 6 . Due to the dynamic evolution of the geometrical structure of coordinated Na-PC/FEC complexes during AIMD simulation, the energy band fluctuates. Thus, 100 structures are sampled from AIMD simulation and 13 NaClO_4 -PC complexes and 24 NaClO_4 -FEC complexes are identified with unrepeated coordination configurations from these obtained structures, as shown in Figures S17 and S18, Supporting Information. Moreover, based on these structures (Figures S19 and S20, Supporting Information), frontier molecule orbital theory was employed to analyze the variation of the lowest unoccupied molecule orbital (LUMO) and HOMO after solvation. The LUMOs and HOMOs of isolated PC, FEC, and NaClO_4 molecules were also calculated as references. From Figure 5b, the HOMOs of both FEC- NaClO_4 complexes and PC- NaClO_4 complexes are

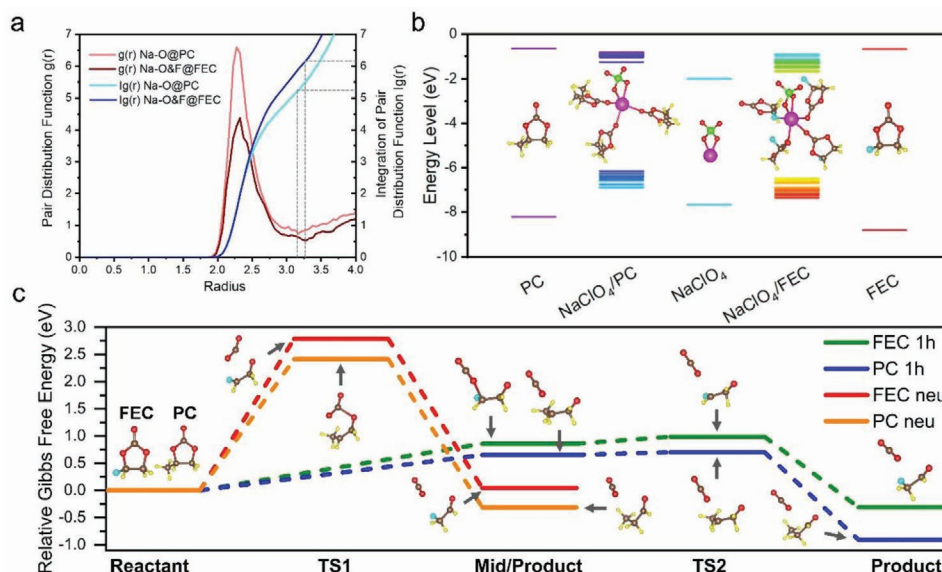


Figure 5. Simulation results based on DFT combined with AIMD. a) The paired distribution functions between Na atoms and O atoms in PC, and between Na atoms and O and F atoms together in FEC, respectively. b) Frontier molecular orbital theory analysis for the FEC–NaClO₄ complexes and PC–NaClO₄ complexes, compared with single molecule. The brown, red, yellow, purple, green, and light blue balls are denoted as carbon atoms, oxygen atoms, hydrogen atoms, sodium atoms, chlorine atoms, and fluorine atoms, respectively. c) The Gibbs energy change of the dissociation reactions of PC and FEC molecules with one electron hole injection or under neutral condition.

up-shifted and the LUMOs are down-shifted, compared with those of isolated PC and FEC molecules. This indicates that the solvation with NaClO₄ reduces the electrolyte stability on both cathode and anode sides. And the lower HOMO of the FEC–NaClO₄ complexes than that of PC–NaClO₄ complexes is suggestive of the superior oxidative stability of the FEC electrolyte. In addition, the calculation of the charge differential density also showed that the solvation effect made the PC/FEC molecules easy to lose electrons, as shown in Figure S21, Supporting Information.

Furthermore, the dissociation energy barriers of PC and FEC molecules under cathodic charged condition were also calculated to get a better understanding of the dynamic factors of their decomposition on the cathode side. Many possible pathways were reported for the oxidative decomposition reaction previously, and the energy-favored pathway with the formation of CO₂ was considered in this work.^[36,37] From Gibbs energy change of the decomposition reaction path (Figure 5c), the decomposition reactions have a relatively large barrier at neutral condition, which is 2.78 eV for FEC and 2.41 eV for PC, respectively. The interaction between FEC and PC molecules and the cathode can be simulated by injecting one electron hole into the system, and the dissociation energy barriers become much lower, 0.98 eV for FEC and 0.70 eV for PC. In addition, the reaction becomes exothermic under the cathodic condition, which is energetically favorable. These results suggest that PC molecules are less stable than FEC molecules on the cathode side, and thus undergo severe decomposition.

The feasibility of using the FEC electrolyte in full cell by pairing Na_{2/3}Ni_{1/3}Mn_{2/3}O₂ cathode with commercial hard carbon anode was demonstrated, as illustrated in Figure 6a; and the cell with PC electrolyte was also tested as reference. Figure 6b shows the cycle stability of the full cells cycled at

5 C (i.e., 400 mA g⁻¹ based on cathode mass) within a voltage range of 2.0–3.8 V. The full cells in FEC electrolyte maintain a capacity retention of 94% after 1000 cycles, whereas only 10% of the initial capacity is retained in PC electrolyte. Meanwhile, the full cells in the FEC electrolyte also deliver superior rate capability and smaller polarization than those in PC electrolyte (Figure 6c–e), which are consistent with the half-cell results. Since the electrolyte has minor effect on the electrochemical performance of the hard carbon anode based on results in half cells (Figure S22, Supporting Information), the improvement in the full cell performance is ascribed to the cathode side.

3. Conclusion

In summary, the rate capability and long-term cycle stability of Na_{2/3}Ni_{1/3}Mn_{2/3}O₂ cathode can be remarkably improved by adopting FEC electrolyte, as oppose to common carbonate-based electrolytes. The FEC electrolyte is revealed to be more stable against oxidation, inducing a robust fluorinated CEI that effectively passivates the surface of Na_{2/3}Ni_{1/3}Mn_{2/3}O₂ cathodes, and thus enabling the substantially enhanced electrochemical performance. Furthermore, simulations based on DFT and AIMD confirm that solvation with NaClO₄ affects the stability of the FEC and PC molecules, and the FEC molecules are more stable on the cathode side because of their lower HOMO energy and higher dissociation energy barriers. By using FEC electrolyte, Na_{2/3}Ni_{1/3}Mn_{2/3}O₂ cathodes deliver outstanding rate capability and cycle stability, that is, 86% capacity utilization as the current density is increased from 0.2–30 C, and 87% capacity retention after 2000 cycles at 5 C. In full cells coupled with a commercial hard carbon anode, 88% capacity utilization is achieved as the current intensity

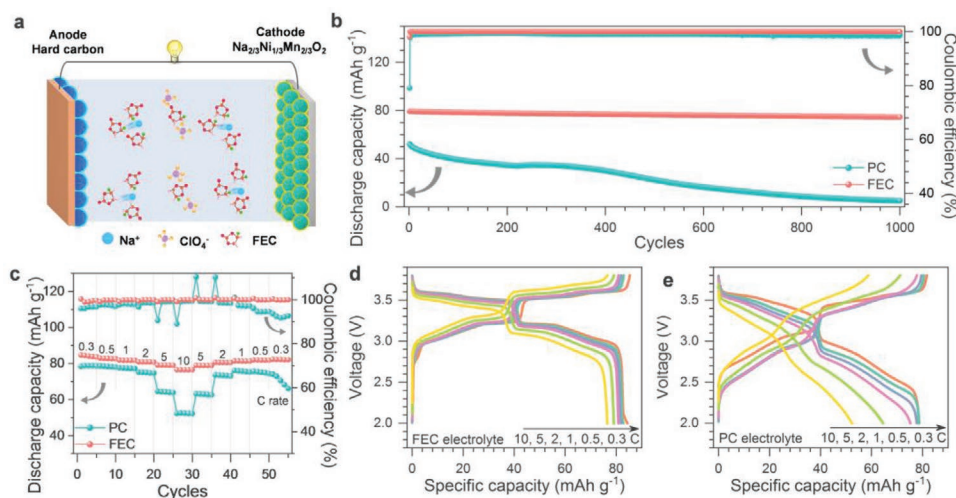


Figure 6. Electrochemical performance of $\text{Na}_{2/3}\text{Ni}_{1/3}\text{Mn}_{2/3}\text{O}_2$ -hard carbon full batteries. a) Schematics of the $\text{Na}_{2/3}\text{Ni}_{1/3}\text{Mn}_{2/3}\text{O}_2$ -hard carbon full cell. b) Cycle performance of the full cells with the FEC electrolyte and PC electrolyte at 5 C ($1\text{ C} = 80\text{ mA g}^{-1}$, based on the mass of cathode materials). c) Rate performance of the full cells with the FEC electrolyte and PC electrolyte. d,e) Charge–discharge curves of the full cells with FEC (d) and PC (e) electrolytes.

is increased from 0.3 to 10 C, and 94% capacity retention is obtained after 1000 cycles at 5 C. These results further validate the feasibility of using FEC electrolyte for practical applications. This work highlights the importance of the electrolyte solvent and the associated CEI formation on the long-term cycle stability of cathodes, which is essential for developing high performance SIBs toward low-cost and durable grid-scale energy storage system.

Supporting Information

Supporting Information is available from the Wiley Online Library or from the author.

Acknowledgements

S.W., B.S., and K.N. contributed equally to this work. The authors are grateful for financial support from the General Research Fund (GRF CityU 11307619 and CityU 11304518), the National Science Foundation of China (51872249, 51672230, 51772282, and 51972299), the China Postdoctoral Science Foundation (2019TQ0306), and funding from Hefei Center for Physical Science and Technology.

Conflict of Interest

The authors declare no conflict of interest.

Keywords

cathode–electrolyte interfaces, density functional simulations, fluoroethylene carbonate, sodium-ion batteries, transitional metal oxides

Received: August 26, 2020

Revised: December 6, 2020

Published online: December 28, 2020

- [1] B. Dunn, H. Kamath, J.-M. Tarascon, *Science* **2011**, 334, 928.
- [2] D. Kundu, E. Talaie, V. Duffort, L. F. Nazar, *Angew. Chem., Int. Ed.* **2015**, 54, 3431.
- [3] N. Yabuuchi, M. Kajiyama, J. Iwatate, H. Nishikawa, S. Hitomi, R. Okuyama, R. Usui, Y. Yamada, S. Komaba, *Nat. Mater.* **2012**, 11, 512.
- [4] H. J. Kim, A. Konarov, J. H. Jo, J. U. Choi, K. Ihm, H. K. Lee, J. Kim, S. T. Myung, *Adv. Energy Mater.* **2019**, 9, 1901181.
- [5] M. Sathiy, K. Hemalatha, K. Ramesha, J. M. Tarascon, A. S. Prakash, *Chem. Mater.* **2012**, 24, 1846.
- [6] Y. Lei, X. Li, L. Liu, G. Ceder, *Chem. Mater.* **2014**, 26, 5288.
- [7] E. Talaie, V. Duffort, H. L. Smith, B. Fultz, L. F. Nazar, *Energy Environ. Sci.* **2015**, 8, 2512.
- [8] U. Maitra, R. A. House, J. Somerville, N. Tapia-Ruiz, J. G. Lozano, N. Guerrini, R. Hao, K. Luo, L. Y. Jin, M. A. Perez-Osorio, F. Massel, D. M. Pickup, S. Ramos, X. Y. Lu, D. E. McNally, A. V. Chadwick, F. Giustino, T. Schmitt, L. C. Duda, M. R. Roberts, P. G. Bruce, *Nat. Chem.* **2018**, 10, 288.
- [9] R. Berthelot, D. Carlier, C. Delmas, *Nat. Mater.* **2011**, 10, 74.
- [10] Y. Jiang, S. Yu, B. Wang, Y. Li, W. Sun, Y. Lu, M. Yan, B. Song, S. Dou, *Adv. Funct. Mater.* **2016**, 26, 5315.
- [11] L. Wang, Y. Lu, J. Liu, M. Xu, J. Cheng, D. Zhang, J. B. Goodenough, *Angew. Chem., Int. Ed.* **2013**, 52, 1964.
- [12] Y. You, X.-L. Wu, Y.-X. Yin, Y.-G. Guo, *Energy Environ. Sci.* **2014**, 7, 1643.
- [13] J. Kim, D.-H. Seo, H. Kim, I. Park, J.-K. Yoo, S.-K. Jung, Y.-U. Park, W. A. Goddard III, K. Kang, *Energy Environ. Sci.* **2015**, 8, 540.
- [14] J. Lu, S. C. Chung, S.-i. Nishimura, A. Yamada, *Chem. Mater.* **2013**, 25, 4557.
- [15] W. Luo, M. Allen, V. Raju, X. Ji, *Adv. Energy Mater.* **2014**, 4, 1400554.
- [16] K. Sakaushi, E. Hosono, G. Nickerl, T. Gemming, H. Zhou, S. Kaskel, J. Eckert, *Nat. Commun.* **2013**, 4, 1485.
- [17] S. W. Wang, L. J. Wang, Z. Q. Zhu, Z. Hu, Q. Zhao, J. Chen, *Angew. Chem., Int. Ed.* **2014**, 53, 5892.
- [18] Q. N. Liu, Z. Hu, M. Z. Chen, C. Zou, H. L. Jin, S. Wang, Q. F. Gu, S. L. Chou, *J. Mater. Chem. A* **2019**, 7, 9215.
- [19] Y. Sun, S. H. Guo, H. S. Zhou, *Energy Environ. Sci.* **2019**, 12, 825.
- [20] P. F. Wang, Y. You, Y. X. Yin, Y. S. Wang, L. J. Wan, L. Gu, Y. G. Guo, *Angew. Chem., Int. Ed.* **2016**, 55, 7445.
- [21] E. Talaie, S. Y. Kim, N. Chen, L. F. Nazar, *Chem. Mater.* **2017**, 29, 6684.

- [22] Y. Xiao, Y. F. Zhu, H. R. Yao, P. F. Wang, X. D. Zhang, H. L. Li, X. N. Yang, L. Gu, Y. C. Li, T. Wang, Y. X. Yin, X. D. Guo, B. H. Zhong, Y. G. Guo, *Adv. Energy Mater.* **2019**, *9*, 1803978.
- [23] K. Kaliyappan, J. Liu, B. W. Xiao, A. Lushington, R. Y. Li, T. K. Sham, X. L. Sun, *Adv. Funct. Mater.* **2017**, *27*, 1701870.
- [24] Y. C. Liu, Q. Y. Shen, X. D. Zhao, J. Zhang, X. B. Liu, T. S. Wang, N. Zhang, L. F. Jiao, J. Chen, L. Z. Fan, *Adv. Funct. Mater.* **2020**, *30*, 1907837.
- [25] Y. H. Liu, X. Fang, A. Y. Zhang, C. F. Shen, Q. Z. Liu, H. A. Enaya, C. W. Zhou, *Nano Energy* **2016**, *27*, 27.
- [26] J. Alvarado, C. Z. Ma, S. Wang, K. Nguyen, M. Kodur, Y. S. Meng, *ACS Appl. Mater. Interfaces* **2017**, *9*, 26518.
- [27] P. F. Wang, H. R. Yao, X. Y. Liu, Y. X. Yin, J. N. Zhang, Y. Wen, X. Yu, L. Gu, Y.-G. Guo, *Sci. Adv.* **2018**, *4*, eaar6018.
- [28] K. Xu, *Chem. Rev.* **2004**, *104*, 4303.
- [29] K. Xu, *Chem. Rev.* **2014**, *114*, 11503.
- [30] X. Fan, L. Chen, X. Ji, T. Deng, S. Hou, J. Chen, J. Zheng, F. Wang, J. Jiang, K. Xu, C. Wang, *Chem* **2018**, *4*, 174.
- [31] Z. Zhang, L. Hu, H. Wu, W. Weng, M. Koh, P. C. Redfern, L. A. Curtiss, K. Amine, *Energy Environ. Sci.* **2013**, *6*, 1806.
- [32] X. Fan, L. Chen, O. Borodin, X. Ji, J. Chen, S. Hou, T. Deng, J. Zheng, C. Yang, S.-C. Liou, K. Amine, K. Xu, C. Wang, *Nat. Nanotechnol.* **2018**, *13*, 715.
- [33] L. Suo, W. Xue, M. Gobet, S. G. Greenbaum, C. Wang, Y. Chen, W. Yang, Y. Li, J. Li, *Proc. Natl. Acad. Sci. USA* **2018**, *115*, 1156.
- [34] Z. Q. Zhu, Y. X. Tang, Z. S. Lv, J. Q. Wei, Y. Y. Zhang, R. H. Wang, W. Zhang, H. R. Xia, M. Z. Ge, X. D. Chen, *Angew. Chem., Int. Ed.* **2018**, *57*, 3656.
- [35] J. G. Han, J. B. Lee, A. Cha, T. K. Lee, W. Cho, S. Chae, S. J. Kang, S. K. Kwak, J. Cho, S. Y. Hong, N. S. Choi, *Energy Environ. Sci.* **2018**, *11*, 1552.
- [36] L. D. Xing, C. Y. Wang, W. S. Li, M. Q. Xu, X. L. Meng, S. F. Zhao, *J. Phys. Chem. B* **2009**, *113*, 5181.
- [37] L. Xia, B. C. Tang, L. B. Yao, K. Wang, A. Cheris, Y. Y. Pan, S. X. Lee, Y. G. Xia, G. Z. Chen, Z. P. Liu, *ChemistrySelect* **2017**, *2*, 7353.